ENHANCED KNOWLEDGE IN SCIENCES AND TECHNOLOGY
e-ISSN: 2773-6385

EKST

Vol. 5 No. 1 (2025) 18-25
https://publisher.uthm.edu.my/periodicals/index.php/ekst

Analysis Using COMSOL of Forced Convective Heat Transfer Past a Square Diamond Shaped Porous Cylinder

Muhammad Aizat Asri[1], Muhamad Ghazali Kamardan[1]*

[1] *Department of Mathematics and Statistics, Faculty of Applied Sciences and Technology, UTHM Kampus Cawangan Pagoh, Hab Pendidikan Tinggi Pagoh, KM 1, Jalan Panchor, 84600 Pagoh, Muar, Johor, MALAYSIA.*

*Corresponding Author: mghazali@uthm.edu.my
DOI: https://doi.org/10.30880/ekst.2025.05.01.003

Article Info

Received: 30 December 2024
Accepted: 16 January 2025
Available online: 30 July 2025

Keywords

Forced Convection, Heat Transfer, Comsol Multiphysics, Streamlines, Isotherms, Porous Media

Abstract

This study investigates the forced convective heat transfer around a diamond-shaped porous cylinder by using COMSOL software. The dimensionless equations for mass, momentum, and energy were solved to produce streamlines and isotherms. By using a constant Darcy number (10^{-2}) and changing the Reynolds number (Re), the analysis was conducted. The outcomes revealed that the effect on the cylinder was symmetrical at low Re with only a small distortion of the streamlines, meaning that the heat transfer was conduction dominated. As Re grows, the streamlines get stretched, and vortices occur downstream of the cylinder, thus telling us that the heat transfer has moved more to convection. The isotherms with an increased Re caused the thermal plume to become longer, this is a sign of the presence of inertial forces. The temperature at the cylinder surface remained high, though the heat was not the same at the points downstream. These results demonstrate the interaction of flow and heat transfer characteristics, and the finding is expected to be a source of knowledge regarding the forced convection in porous media.

1. Introduction

Many engineering applications consider heat transfer as a key factor in improving thermal performance in systems such as heat exchangers, filtration devices and electronic cooling systems. To improve heat transfer efficiency, forced convection is frequently employed, where fluid motion requires external acceleration to occur at a specific point in time [1]. In such systems, the shape and material properties of the components significantly influence the fluid flow and heat transfer behaviour.

Convective heat transfer mechanisms have been extensively studied in the context of porous media. Studies on heat transfer over cylindrical geometries highlight the influence of fluid properties and Reynolds number (Re) on the Nusselt number (Nu) [2]. Research has also demonstrated that increasing the Darcy number (Da) and porosity enhances heat transfer in porous square cylinders [3]. These findings underscore the importance of dimensionless parameters such as Re, Da, and Nu in characterizing heat transfer in porous systems.

The flow and thermal properties of porous media are different from those of other media because of the permeability of the porosity layers, which are effective for multiple applications. The Darcy-Brinkman equation for this type of system is used to model mass, momentum, and thermal energy transport because it considers the viscosity of the fluid, as well as the permeability of the porous media[4]. Study of porous media pointed out that such systems affect largely the flow fields and thermal characters and provided lower heat transfer rate under some conditions [5,6].

The development and application of numerical tools, particularly COMSOL Multiphysics, have furthered understanding of heat transfer phenomena in complex geometries. Finite element method (FEM)-based studies have been used to investigate forced convection in non-Newtonian fluids and analyse heat transfer in porous aluminium foam [7,8]. These studies confirm that numerical simulations align well with experimental data, validating the reliability of FEM approaches. Previous studies have examined the effects of parameters such as Reynolds number and Darcy number on flow structures and heat transfer efficiency in porous systems [9,10], primarily using finite volume or finite difference methods.

Previous studies prove that finite volume method (FVM) is a suitable technique to predict the flow and heat transfer of fluids across a square diamond shaped porous cylinder. This method seeks to divide the computational area into small control volumes to maintain conservation laws in each segment. To handle the pressure and velocity coupling the SIMPLE algorithm is employed. On the other hand, a second order upwind scheme is used to discretize the convection terms to enhance the simulations of the fluid flow. The Darcy-Brinkman equation is applied to simulate the flow through porous medium, considering with the viscous diminution and permeability of the material. Moreover, the Forchheimer term is included to account for the inertial linear construct for higher flow velocity thus making the approach appropriate to analyse flow and heat transactions within tight structures of porosity [11].

This study however adopts a different approach through employing FEM using COMSOL Multiphysics to study forced convection heat transfer in the same setup. Using relatively small, flexible elements of the region, FEM can effectively reach an approximate result even when considering the complex shapes of the objects and their interactions. Since incompressibility, viscosity, permeability and the contribution of the inertia terms are important, we use the Darcy-Brinkman-Forchheimer model. Moreover, using COMSOL, one can obtain modern solutions to the problems that are not reachable using FVM-based tools: accurate analysis of isotherms and streamlines.

Nomenclature

D	Diameter of the cylinder (m)
Da	Darcy number ($= K/D^2$)
F_d	Drag force (N)
h	Heat transfer coefficient (W/m^2K)
k	Thermal conductivity (W/$m\ K$)
K	Permeability (m^2)
Nu	Nusselt number ($= h\ D/k$)
Nu_{ave}	Average Nusselt number
P	Pressure (Pa)
Pe	Peclet number ($= Re \times Pr$)
Pr	Prandtl number ($= \nu/\alpha$)
q'''	Heat source (W/m^3)
R_c	Thermal conductivity ratio ($= k_{eff}/k_f$)
Re	Reynolds number ($= U_\infty D/\nu$)
t	Time (s)
T	Temperature (K)
x, y	Rectangular coordinates (m)
u, v	Velocity component in x and y directions (ms^{-1})

Greek symbols

α	Thermal diffusivity (m^2s^{-1})
ε	Porosity
μ	Dynamic viscosity ($kg\ m^{-1}s^{-1}$)
ν	Fluid kinematic viscosity (m^2s^{-1})
ρ	Fluid density ($kg\ m^{-3}$)

Enhanced Knowledge in Sciences and Technology Vol. 5 No. 1 (2025) p. 18-25

2. Research Method

As show in Fig. 1, a square diamond-shaped porous cylinder with diameter D is taken into consideration, through which a uniform fluid flows from left to right at a temperature T_∞ and free stream velocity U_∞. The length is 10D and width of the domain is 30D. Heat is produced inside the porous cylinder in this problem. To enable numerical simulations of the problem, the subsequent presumptions are established:

- Two-dimensional steady state laminar flow around and through an isotropic, homogenous porous matrix with uniform and constant porosity is the topic under investigation. Porous cylinder saturated with a single-phase fluid.
- In this case, the body forces are small, and the fluid parameters are taken to be constant.
- According to local thermal equilibrium, the temperature of the fluid phase and the solid phase are identical. When examining heat transmission in porous media, this thermal boundary condition is frequently employed. This presumption is true in situations when there is no temperature difference between the fluid and solid phases. This boundary condition fails when there is a large temperature difference throughout the porous media or when cooling or heating occurs quickly.

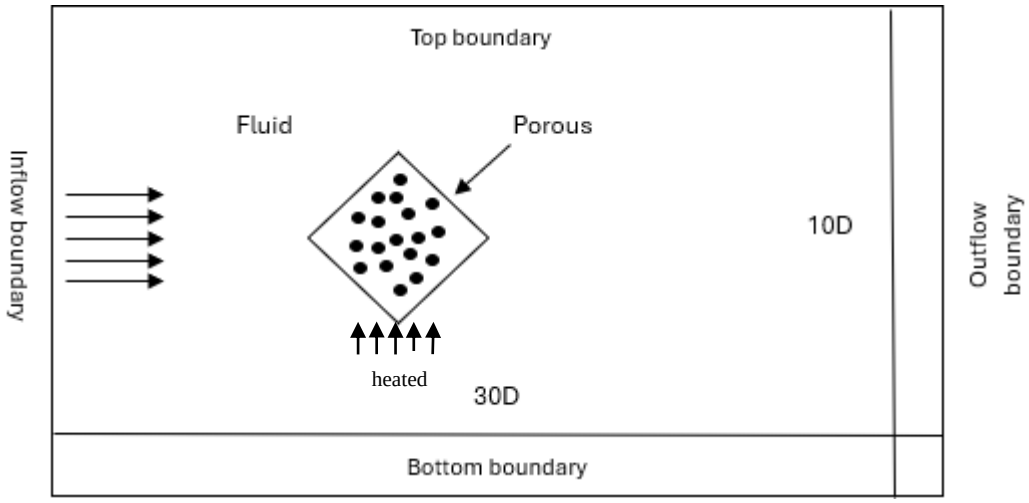

Fig. 1 Computational domain and geometry of squared diamond shaped porous cylinder

The governing equations are shown in equation (1) to (8).

Clear Domain

$$\frac{\partial u_1^*}{\partial x^*} + \frac{\partial v_1^*}{\partial y^*} = 0 \tag{1}$$

$$\rho_f \left(\frac{\partial u_1^*}{\partial t^*} + u_1^* \frac{\partial u_1^*}{\partial x^*} + v_1^* \frac{\partial u_1^*}{\partial y^*}\right) = -\frac{\partial p_1^*}{\partial x^*} + \mu\left(\frac{\partial^2 u_1^*}{\partial x^{*2}} + \frac{\partial^2 u_1^*}{\partial y^{*2}}\right) \tag{2}$$

$$\rho_f \left(\frac{\partial v_1^*}{\partial t^*} + u_1^* \frac{\partial v_1^*}{\partial x^*} + v_1^* \frac{\partial v_1^*}{\partial y^*}\right) = -\frac{\partial p_1^*}{\partial y^*} + \mu\left(\frac{\partial^2 v_1^*}{\partial x^{*2}} + \frac{\partial^2 v_1^*}{\partial y^{*2}}\right) \tag{3}$$

$$\rho_f c_p \left(\frac{\partial T_1^*}{\partial t^*} + u_1^* \frac{\partial T_1^*}{\partial x^*} + v_1^* \frac{\partial T_1^*}{\partial y^*}\right) = k_f\left(\frac{\partial^2 T_1^*}{\partial x^{*2}} + \frac{\partial^2 T_1^*}{\partial y^{*2}}\right) \tag{4}$$

Porous Domain

$$\frac{\partial u_2^*}{\partial x^*} + \frac{\partial v_2^*}{\partial y^*} = 0 \tag{5}$$

$$\frac{\rho_f}{\varepsilon^2}\left(\varepsilon\frac{\partial u_2^*}{\partial t^*} + u_2^* \frac{\partial u_2^*}{\partial x^*} + v_2^* \frac{\partial u_2^*}{\partial y^*}\right) = -\frac{\partial p_2^*}{\partial x^*} + \frac{\mu}{\varepsilon}\left(\frac{\partial^2 u_2^*}{\partial x^{*2}} + \frac{\partial^2 u_2^*}{\partial y^{*2}}\right) - \frac{\mu}{K}u_2^* - \frac{C_F \rho_f}{\sqrt{K}}\left(\sqrt{u_2^{*2} + v_2^{*2}}\right)u_2^* \tag{6}$$

$$\frac{\rho_f}{\varepsilon^2}\left(\varepsilon\frac{\partial v_2^*}{\partial t^*} + u_2^* \frac{\partial v_2^*}{\partial x^*} + v_2^* \frac{\partial v_2^*}{\partial y^*}\right) = -\frac{\partial p_2^*}{\partial y^*} + \frac{\mu}{\varepsilon}\left(\frac{\partial^2 v_2^*}{\partial x^{*2}} + \frac{\partial^2 v_2^*}{\partial y^{*2}}\right) - \frac{\mu}{K}v_2^* - \frac{C_F \rho_f}{\sqrt{K}}\left(\sqrt{u_2^{*2} + v_2^{*2}}\right)v_2^* \tag{7}$$

$$\frac{\rho_f c_p}{\varepsilon}\left(\varepsilon\frac{\partial T_2^*}{\partial t^*} + u_2^* \frac{\partial T_2^*}{\partial x^*} + v_2^* \frac{\partial T_2^*}{\partial y^*}\right) = k_{eff}\left(\frac{\partial^2 T_2^*}{\partial x^{*2}} + \frac{\partial^2 T_2^*}{\partial y^{*2}}\right) + q''' \tag{8}$$

The equations (1) to (8) were converted into dimensionless forms by using the following dimensionless variables conductivity ratio parameter, Darcy number, Reynolds number, Prandtl number, and Péclet number, respectively.

$$x = \frac{x^*}{D}, y = \frac{y^*}{D}, u = \frac{u^*}{U_\infty}, v = \frac{v^*}{U_\infty}, p = \frac{p^*}{\rho U_\infty^2}, t = \frac{t^* U_\infty}{D}, T = \frac{T^* - T_\infty}{q''' D^2/k_f}$$
$$R_c = \frac{k_{eff}}{k_f}, Da = \frac{K}{D^2}, Re = \frac{\rho U_\infty D}{\mu}, Pr = \frac{v}{\alpha}, Pe = RePr \quad (9)$$

The crucial and important elements in this study are Darcy number (Da) and Reynolds number (Re). The symbols α, v, and ρ which stand for thermal diffusivity, kinematic viscosity, and fluid density, respectively. Next, permeability and temperature are represented by K and T while x, y represent the rectangular coordinates and velocity components in the x and y directions stand for u and v. We created the dimensionless equation by substituting the scaling parameter in accordance with the conservation of mass equation in clear domain.
By using the variables in equation (9), equations (1)-(8) are converted to equation (10) to (17).

Clear Domain

$$\frac{\partial u_1}{\partial x} + \frac{\partial v_1}{\partial y} = 0 \quad (10)$$
$$\frac{\partial u_1}{\partial t} + u_1\frac{\partial u_1}{\partial x} + v_1\frac{\partial u_1}{\partial y} = -\frac{\partial p_1}{\partial Dx} + \frac{1}{Re}\left(\frac{\partial^2 u_1}{\partial x^2} + \frac{\partial^2 u_1}{\partial y^2}\right) \quad (11)$$
$$\frac{\partial v_1}{\partial t} + u_1\frac{\partial v_1}{\partial x} + v_1\frac{\partial v_1}{\partial y} = -\frac{\partial p_1}{\partial Dy} + \frac{1}{Re}\left(\frac{\partial^2 v_1}{\partial x^2} + \frac{\partial^2 v_1}{\partial y^2}\right) \quad (12)$$
$$\frac{\partial T_1}{\partial t} + u_1\frac{\partial T_1}{\partial x} + v_1\frac{\partial T_1}{\partial y} = \frac{1}{Pe}\left(\frac{\partial^2 T_1}{\partial x^2} + \frac{\partial^2 T_1}{\partial y^2}\right) \quad (13)$$

Porous Domain

$$\frac{\partial u_2}{\partial x} + \frac{\partial v_2}{\partial y} = 0 \quad (14)$$
$$\frac{1}{\varepsilon^2}\left(\varepsilon\frac{\partial u_2}{\partial t} + u_2\frac{\partial u_2}{\partial x} + v_2\frac{\partial u_2}{\partial y}\right) = -\frac{\partial p_2}{\partial x} + \frac{1}{\varepsilon Re}\left(\frac{\partial^2 u_2}{\partial x^2} + \frac{\partial^2 u_2}{\partial y^2}\right) - \frac{1}{ReDa}(u_2) - \frac{C_f}{\sqrt{Da}}\left(\sqrt{u_2^2 + v_2^2}\right)u_2 \quad (15)$$
$$\frac{1}{\varepsilon^2}\left(\varepsilon\frac{\partial v_2}{\partial t} + u_2\frac{\partial v_2}{\partial x} + v_2\frac{\partial v_2}{\partial y}\right) = -\frac{\partial p_2}{\partial y} + \frac{1}{\varepsilon Re}\left(\frac{\partial^2 v_2}{\partial x^2} + \frac{\partial^2 v_2}{\partial y^2}\right) - \frac{1}{ReDa}(v_2) - \frac{C_f}{\sqrt{Da}}\left(\sqrt{u_2^2 + v_2^2}\right)v_2 \quad (16)$$
$$\frac{1}{\varepsilon}\left(\varepsilon\frac{\partial T_2}{\partial t} + u_2\frac{\partial T_2}{\partial x} + v_2\frac{\partial T_2}{\partial y}\right) = \frac{Rc}{Pe}\left(\frac{\partial^2 T_2}{\partial x^2} + \frac{\partial^2 T_2}{\partial y^2}\right) + \frac{1}{Pe} \quad (17)$$

The boundary conditions are as follows:

Inlet section (Uniform flow)

$$u_1 = 1, v_1 = 0, T_1 = 0$$

Upper and lower boundaries (Frictionless wall and zero Heat flux)

$$\frac{\partial u_1}{\partial y} = 0, v_1 = 0, \frac{\partial T_1}{\partial y} = 0$$

Outlet boundary (Neumann boundary conditions are applied for both velocity and temperature fields)

Enhanced Knowledge in Sciences and Technology Vol. 5 No. 1 (2025) p. 18-25

Interface Between Fluid and Porous Regions:
Continuity of velocity, temperature, and heat flux at the interface is enforced using the following conditions:

$$u_1 = u_{2,}\, v_1 = v_2$$

$$\mu_f \frac{\partial u_1}{\partial y} = \mu_{eff} \frac{\partial u_2}{\partial y}$$

$$T_1 = T_2$$

$$\frac{\partial T_1}{\partial x} = R_c \frac{\partial T_2}{\partial x}, \frac{\partial T_1}{\partial y} = R_c \frac{\partial T_2}{\partial y}$$

where R_c is the thermal conductivity ratio, μ_f is the fluid viscosity, and μ_{eff} is the effective viscosity in the porous medium.

3. Results and Discussion

To validate the accuracy of the study, the results of numerical simulations on forced convective heat transfer past a diamond-shaped porous cylinder using COMSOL Multiphysics are presented. The study examines the behaviour of fluid flow and heat transfer in the presence of a porous obstacle under varying Reynolds numbers (Re) and Darcy numbers (Da) is fixed at 10^{-2}. The findings are demonstrated using streamline contours, isotherm distributions, and quantitative metrics to highlight the impact of these parameters on flow and thermal characteristics. Increasing Re enhances convective heat transfer, reduces thermal boundary layer thickness, and alters recirculation zones, while higher Da improves permeability, allowing greater fluid penetration and better heat dissipation.

3.1 Streamlines

Fig. 2 illustrates the streamline patterns for a fixed Darcy number of 10^{-2} and different Reynolds numbers: (a) Re = 1, (b) Re = 20, and (c) Re = 40. The colour gradient represents the velocity distribution, with distinct regions of flow behaviour. The blue region corresponds to areas of slower flow, particularly near the porous cylinder where the flow interacts with the porous medium. In contrast, the green to red regions indicates areas of higher velocity as the flow accelerates around the edges of the porous cylinder.

In Fig. 2(a), the streamlines demonstrate a smooth and symmetrical flow around the square diamond-shaped porous region at Re = 1. The flow, dominated by viscous forces, exhibits tightly packed streamlines near the porous shape, with minimal separation or recirculation zones. The colour gradient transitions smoothly, reflecting steady and predictable flow behaviour typical at low Reynolds numbers. The porous region influences the flow distribution by causing localized areas of reduced velocity (blue regions) and smoother transitions to higher velocities (green to red) in the surrounding fluid.

In Fig. 2(b), the streamlines show a laminar flow pattern around the porous cylinder at Re = 20. The flow is influenced by both viscous and inertial forces, with viscous forces still having a strong effect. The streamlines bend smoothly around the cylinder, creating a small and balanced wake region behind it. The colour gradient represents the flow velocity, with blue indicating slower speeds (in the wake and stagnant zones) and red indicating faster speeds (where the flow accelerates). The streamlines are closer together near the cylinder, showing higher velocity changes in this area, while the wake region has slower flow. This pattern highlights how the porous cylinder affects the flow, particularly through the interaction between viscous forces and the obstacle.

In Fig. 2(c), the streamlines show the flow pattern at Re = 40, where inertial forces become more dominant compared to Fig. 2(b). The flow is still laminar but shows less bending and flows more smoothly around the porous cylinder. The colour gradient represents the velocity, with blue indicating slower speeds (in the wake region) and red indicating faster speeds (in areas where the flow accelerates). The wake region behind the cylinder is longer and less symmetrical, showing that inertial forces are now stronger than viscous forces. The streamlines are less tightly packed near the cylinder, indicating smaller velocity changes compared to Re = 20. This pattern shows how the flow behaviour changes as the Reynolds number increases, with the flow becoming more steady and less affected by the porous cylinder.

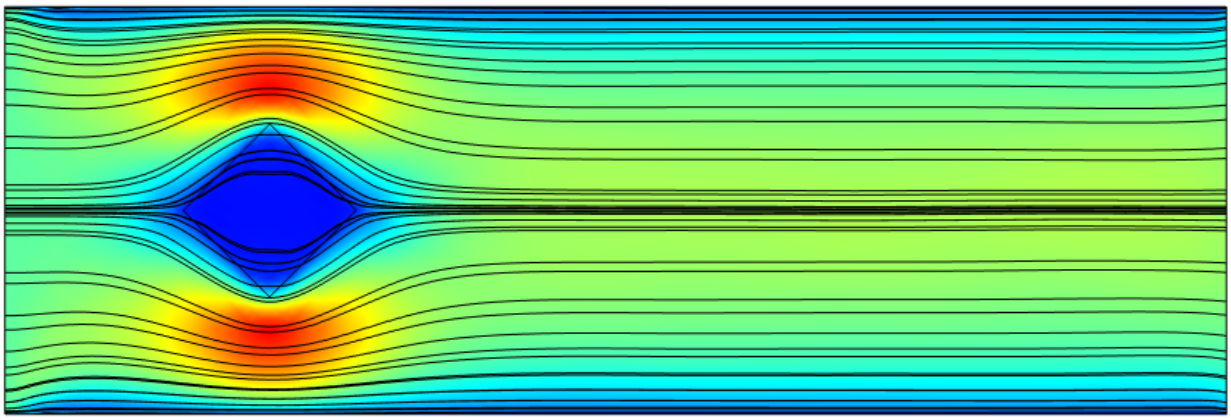

(a)

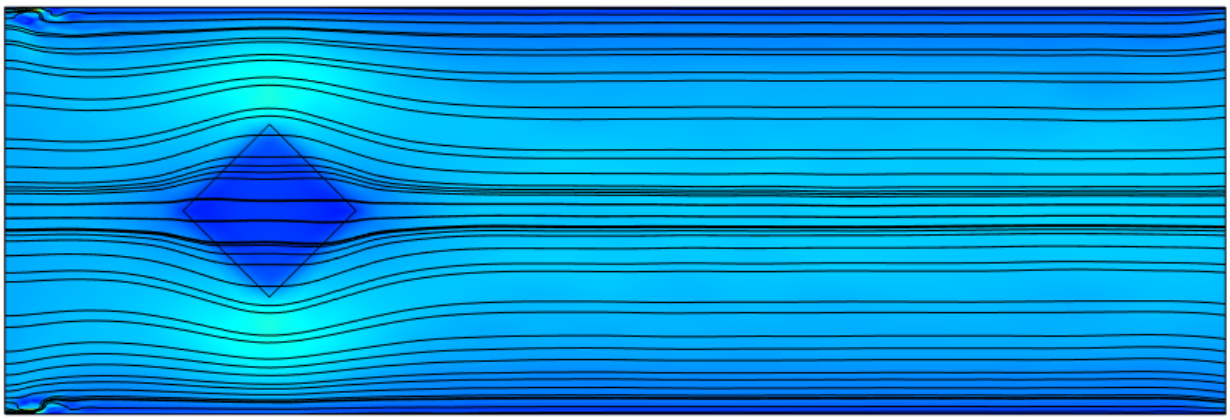

(b)

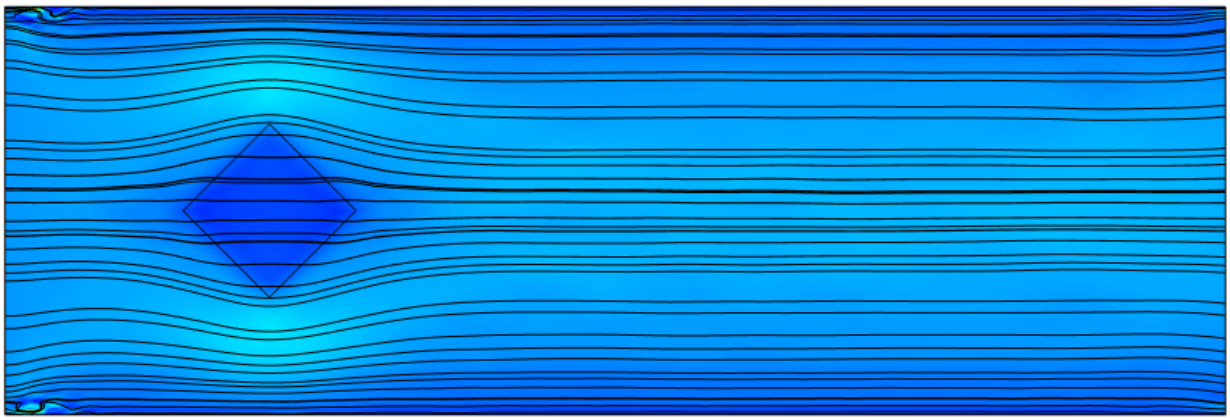

(c)

Fig. 2 streamline at fixed Darcy number, Da = $\mathbf{10^{-2}}$ and different Reynolds numbers, Re: (a) Re = 1, (b) Re = 20, and (c) Re = 40

3.2 Isotherm

Fig. 3 illustrates the isotherm contour for a fixed Darcy number of 10^{-2} and different Reynolds numbers: (a) Re = 1, (b) Re = 20, and (c) Re = 40. Fig. 3(a) shows the isotherms are more uniformly distributed around the square diamond shaped porous region, showing smooth and symmetric patterns. The dominant heat transfer mechanism in this low Re regime is conduction due to the low inertial effects. The temperature values near the diamond's surface are high, reaching approximately 48.04°C, while further away from the region, the temperature decreases gradually to around 12.67°C. The close spacing of the isotherms near the porous region indicates a strong thermal gradient, while the smooth, elongated isotherm contours downstream reflect a steady heat dissipation into the surrounding flow.

Enhanced Knowledge in Sciences and Technology Vol. 5 No. 1 (2025) p. 18-25

Fig. 3(b) shows the isotherms become more distorted and stretched downstream of the porous region, indicating the increasing influence of convective heat transfer. The higher Re introduces greater inertial effects, causing the heat to spread further downstream. The maximum temperature near the diamond surface remains approximately 48.05°C, like the Re = 1 case, but the thermal gradients downstream are more pronounced. The temperature values range from 12.86°C to 44.14°C in regions closer to the diamond region. The isotherm contours are less symmetric compared to Re = 1, reflecting the stronger convective forces dominating heat transfer at this higher Re.

Fig. 3(c) shows the isotherms are elongated and noticeably stretched downstream from the porous region. This indicates the dominance of convective heat transfer, as the inertial effects are stronger compared to lower Re values. The temperature near the surface of the square diamond shaped porous cylinder reaches a maximum of 48.06°C, while the lowest temperature in the domain is approximately 13.21°C. Key temperature values in the flow include 44.19°C, 40.32°C, 36.45°C, 28.70°C, and 20.96°C, showing a gradual decrease as the heat spreads further downstream. The contours become less symmetric compared to lower Reynolds numbers, highlighting the stronger influence of inertial forces at higher Re. This results in greater heat dissipation, as the convective forces dominate over conduction, leading to a longer and more dispersed thermal plume extending into the flow field.

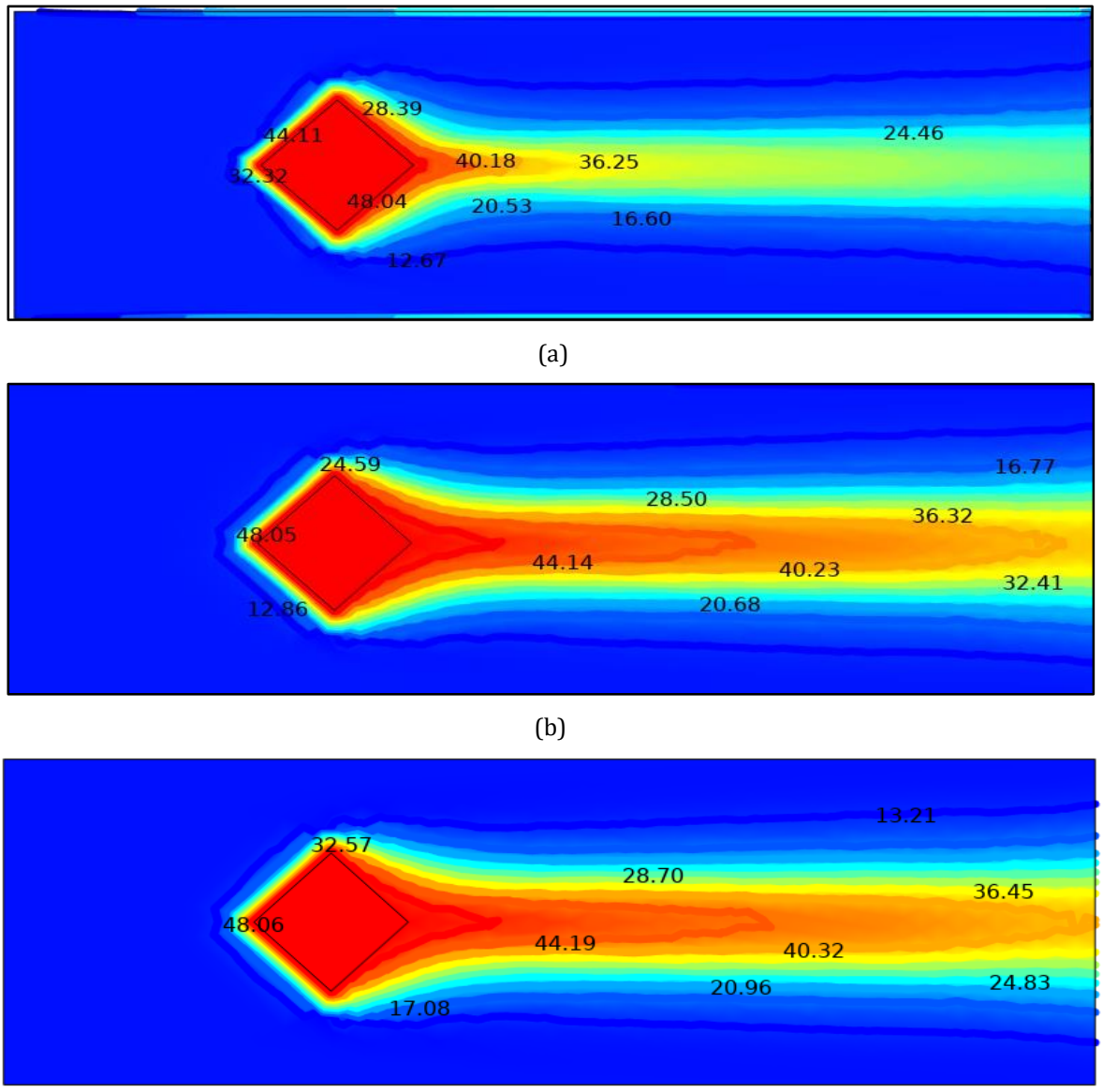

Fig. 3 *isotherm for fixed Darcy number, Da =* $\mathbf{10^{-2}}$ *and different Reynolds number, Re: (a) Re = 1, (b) Re = 20, and (c) Re = 40*

4. Conclusion

In summary, this study used COMSOL to investigate forced convective heat transfer through a square diamond-shaped porous cylinder, with an emphasis on analysing the behaviour of streamlines and isotherms within both the fluid and porous zones. By applying the Darcy Brinkman equation and the principles of heat transfer in fluids, the study effectively modelled the distribution of heat, showing how heat is generated within the porous medium and spreads throughout the surrounding fluid. The results highlight the importance of square diamond porous shape and porosity in influencing both the flow and thermal fields. Streamline contours indicated complex flow patterns around the porous structure, with significant alterations in flow velocity near the square diamond shape's surface. Meanwhile, the isotherm contours revealed how heat was transported from the porous region into the surrounding fluid, demonstrating areas of higher thermal gradients near the region.

Several suggestions for further research are made considering the study's findings. It might be beneficial to investigate several shapes. Testing different shapes, such as cylinder or triangular, could shed further light on how geometry influences flow behaviour and heat transmission. It would also be beneficial to investigate the effects of different porosity levels on heat transfer. Varying porosity levels may provide new methods to enhance thermal performance.

Acknowledgement

The authors would like to thank the Faculty of Applied Sciences and Technology, Universiti Tun Hussein Onn Malaysia for its support.

Conflict of Interest

Authors declare that there is no conflict of interests regarding the publication of the paper.

Author Contribution

The authors confirm contribution to the paper as follows: ***study conception and design:*** *Muhammad Aizat Asri;* ***solve the governing equation:*** *Muhammad Aizat Asri;* ***analysis and interpretation of results:*** *Muhammad Aizat Asri, Muhamad Ghazali Kamardan;* ***draft manuscript preparation:*** *Muhammad Aizat Asri, Muhamad Ghazali Kamardan. All authors reviewed the results and approved the final version of the manuscript.*

References

[1] Zohuri B. (2017). *Heat transfer physics*. Springer.
[2] Mandhani R, Mahajan R, Sharma A. (2001). Forced convection heat transfer over cylindrical geometries. *International Journal of Heat and Mass Transfer*;44:2165–75.
[3] Perng Y, Lee S, Lee M. (2011). Heat transfer in porous square cylinders. *Applied Thermal Engineering*;31:234–42.
[4] Rashidi S, Jafari M, Soleimani A. (2014). Flow and thermal characteristics in porous media. *Transport in Porous Media*;104:245–67.
[5] Layeghi M, Moradi S, Javan M. (2006). Convective heat transfer in porous media. *Numerical Heat Transfer*;49:512–24.
[6] Mahdaoui M, Mansouri A, Kharfi A. (2017). Analysis of flow and heat transfer using the Darcy-Brinkman model. *Energy Conversion and Management*;141:240–9.
[7] Sreenivasulu G, Venkatachari S, Rajasekhar R. (2014). FEM analysis of forced convection in non-Newtonian fluids. *Numerical Methods in Fluid Dynamics*;25:345–57.
[8] Boulahrouz S, Benzaoui A, Imine B. (2017). Heat transfer in porous aluminum foam. *Applied Energy*;187:300–11.
[9] Revnic C, Pop I, Ingham D. (2011). Magnetic field effects on convection in porous enclosures. *Journal of Magnetism and Magnetic Materials*;323:1813–22.
[10] Sathiyamoorthy D, Chamkha AJ. (2012). Magnetic field influence on natural convection. *International Journal of Heat and Fluid Flow*;33:432–45.
[11] Rashidi S, Bovand M, Pop I, Valipour MS. (2014). Numerical Simulation of Forced Convective Heat Transfer Past a Square Diamond-Shaped Porous Cylinder. Transp Porous Media; 102: 207–225.